Available online at www.sciencedirect.com
SCIENCE DIRECT®
Journal of Power Sources 119–121 (2003) 511–516
JOURNAL OF POWER SOURCES
www.elsevier.com/locate/jpowsour

Diagnosis of power fade mechanisms in high-power lithium-ion cells☆

D.P. Abraham[a,*], J. Liu[a], C.H. Chen[a], Y.E. Hyung[a], M. Stoll[a], N. Elsen[a], S. MacLaren[b], R. Twesten[b], R. Haasch[b], E. Sammann[b], I. Petrov[b], K. Amine[a], G. Henriksen[a]

[a]*Argonne National Laboratory, Chemical Technology Division, Argonne, IL 60439, USA*
[b]*Center for Microanalysis of Materials, University of Illinois at Urbana–Champaign, Urbana, IL 61801, USA*

Abstract

Hybrid electric vehicles (HEV) need long-lived high-power batteries as energy storage devices. Batteries based on lithium-ion technology can meet the high-power goals but have been unable to meet HEV calendar-life requirements. As part of the US Department of Energy's Advanced Technology Development (ATD) Program, diagnostic studies are being conducted on 18650-type lithium-ion cells that were subjected to accelerated aging tests at temperatures ranging from 40 to 70 °C. This article summarizes data obtained by gas chromatography, liquid chromatography, electron microscopy, X-ray spectroscopy and electrochemical techniques, and identifies cell components that are responsible for the observed impedance rise and power fade.

Keywords: Calendar-life; Chromatography; Microscopy; Spectroscopy

1. Introduction

High-power lithium-ion batteries are promising alternatives to the nickel metal hydride batteries currently used for energy storage in hybrid electric vehicles (HEV). Commercialization of lithium-ion batteries is, however, limited by calendar-life performance, thermal abuse characteristics, and cost. The Advanced Technology Development (ATD) Program was established by the US Department of Energy to address these limitations. An important objective of this program is the development and application of diagnostic tools that provide unique ways to investigate the phenomena that limit lithium-ion cell life and performance.

As part of the ATD program, accelerated aging and thermal abuse tests were conducted on cylindrically wound (18650-type) ~1 Ah capacity cells fabricated by an industrial manufacturer using a high-power multi-tab design. In the baseline (Gen 1) cells, the positive electrode laminates comprised a ~40 μm coating containing 84 wt.% $LiNi_{0.8}Co_{0.2}O_2$, 4 wt.% SFG-6 graphite, 4 wt.% acetylene black, and 8 wt.% polyvinylidene fluoride (PVdF) binder on a 20 μm thick Al foil. The negative electrode laminates comprised a ~40 μm coating containing 75 wt.% MCMB-6 graphite, 17 wt.% SFG-6 graphite, and 8 wt.% PVdF binder on a 12 μm thick Cu foil. A 37 μm thick three-layer polymer membrane was used as the separator, and the electrolyte was 1 M $LiPF_6$ in ethylene carbonate (EC):diethyl carbonate (DEC) (1:1 wt.%) solvent.

The Gen 1 cells that were subjected only to formation cycles met the high-power performance criteria established for HEV energy storage systems [1]. The cells, however, lost a significant portion of their high-power capability during prolonged storage at fixed voltages (3.6–3.92 V) at temperatures ranging from 40 to 70 °C; the rate of power loss was greater for cells held at the higher voltages and higher test temperatures [2]. The rate of power loss was also higher for cells that were cycled about the nominal voltage according to a defined profile that consisted of charge and discharge pulses. In addition, the power loss values for the cells were two to five times greater than the corresponding capacity loss values.

Various diagnostic tools helped determine the nature and extent of physical, chemical, and structural changes in cell components that resulted from the aging tests [3–8]. This article summarizes the results of diagnostic examinations conducted at Argonne National Laboratory (ANL) and at the University of Illinois at Urbana–Champaign (UIUC). Reference electrode (RE) and symmetric cell studies were conducted to identify positive and negative electrode con-

☆ The submitted manuscript has been created by the University of Chicago as Operator of Argonne National Laboratory ("Argonne") under Contract No. W-31-109-ENG-38 with the US Department of Energy. The US Government retains for itself, and others acting on its behalf, a paid-up, non-exclusive, irrevocable world-wide license in said article to reproduce, prepare derivative works, distribute copies to the public, and perform publicly and display publicly, by or on behalf of the Government.

* Corresponding author. Tel.: +1-630-252-4332; fax: +1-630-972-4406.
E-mail address: abraham@cmt.anl.gov (D.P. Abraham).

0378-7753/03/$ – see front matter © 2003 Elsevier Science B.V. All rights reserved.
doi:10.1016/S0378-7753(03)00275-1

tributions to the impedance rise. Electrode and separator materials were characterized by microscopy and spectroscopy techniques to determine the extent of aging-induced material degradation. Electrolyte changes and gases generated during cell aging were monitored to identify electrode–electrolyte reactions. These data will guide the development of future lithium-ion cell designs and chemistries.

2. Experimental techniques

Cells were discharged to ~3.1 V after test completion. A cell-puncture/gas-collection fixture was used to collect and to determine gas volumes in the cells. Gas composition was determined using He carrier gas with a Hewlett-Packard (HP) 6890 series gas chromatograph. A thermal conductivity detector was used to study non-combustible gases and a HP 5973 mass selective detector was used to study hydrocarbon gases. The punctured cells were centrifuged to extract the electrolyte, which was analyzed by Hitachi D-7000 high-performance liquid chromatograph. The analysis was conducted with a water–acteonitrile (60 vol.%:40 vol.%) mobile phase and a refractive index detector.

Electrode materials studied were from three categories: fresh, control and aged. The fresh samples had no electrolyte contact. The control samples were from cells that underwent formation cycles but were not aged; by definition, the capacity- and power-fade of these cells were zero. The aged samples were from 18650-cells that underwent calendar- and cycle-life tests [2]. Pulse power capability of these cells was calculated from impedance data obtained from the hybrid pulse power characterization test. Increase in cell impedance during aging resulted in loss of cell power, i.e. power fade.

Reference electrode (RE) cells were prepared with 15.5 cm^2 positive and negative materials from the control and aged 18650-cells [6]. The RE was a Li–Sn alloy on the tip of a 25 μm thick Cu wire, which was insulated by a 3 μm thick layer of polyurethane enamel to prevent mixed potentials along the length of the wire. A double-separator configuration isolated the RE from the cell electrodes. Impedance values were calculated from the potential change of each electrode relative to the RE during high-current pulse-charge and discharge measurements.

Symmetric coin cells (1.6 cm^2 electrode area) that contained either two positive or two negative electrodes were prepared to complement reference electrode cell data [5]. A full cell (15.5 cm^2 electrode area), prepared with positive and negative electrode materials from the 18650-cells and charged to a desired voltage, was disassembled to provide materials for the symmetric cells. The ac impedance measurements (0.01 Hz to 100 kHz) were conducted to determine aging-induced changes in the symmetric cells.

An Hitachi S-4700 scanning electron microscope (SEM) and a JEOL 2010F transmission electron microscope (TEM) operating at 200 kV were used to determine changes in material composition and crystal structure. Electrode surfaces were characterized by a Kratos AXIS Ultra X-ray Photoelectron Spectrometer (XPS).

3. Results and discussion

3.1. Electrochemical studies on electrode materials

Representative area specific impedance (ASI) data from RE cells prepared with materials from a control and an aged 18650-cell are shown in Fig. 1. It is evident from the figure

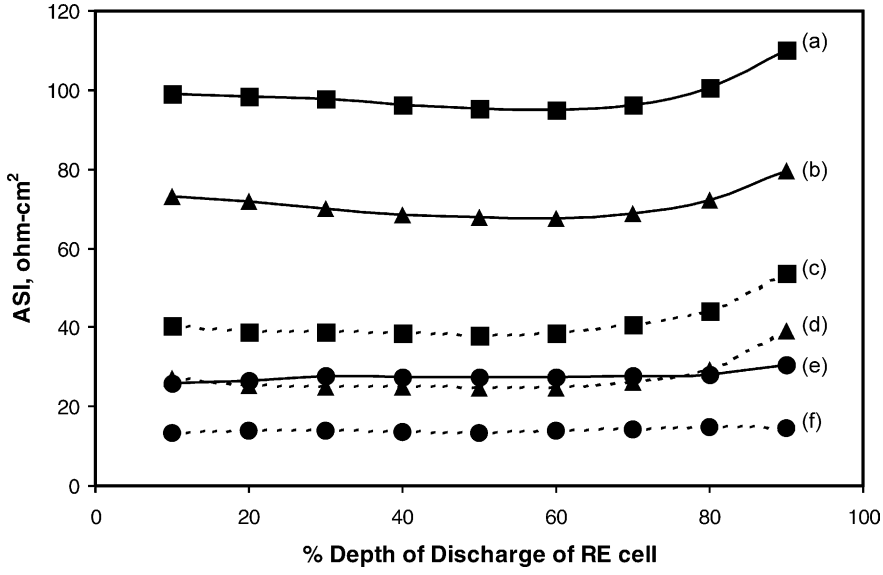

Fig. 1. Area specific impedance (ASI) determined from reference electrode cells prepared from materials obtained from aged (70 °C, 2 weeks) and control (formation only) 18650-cells: (a) aged full cell, (b) aged positive electrode, (c) control full cell, (d) control positive electrode, (e) aged negative electrode and (f) control negative electrode. The ASI increase can be mainly attributed to the positive electrode.

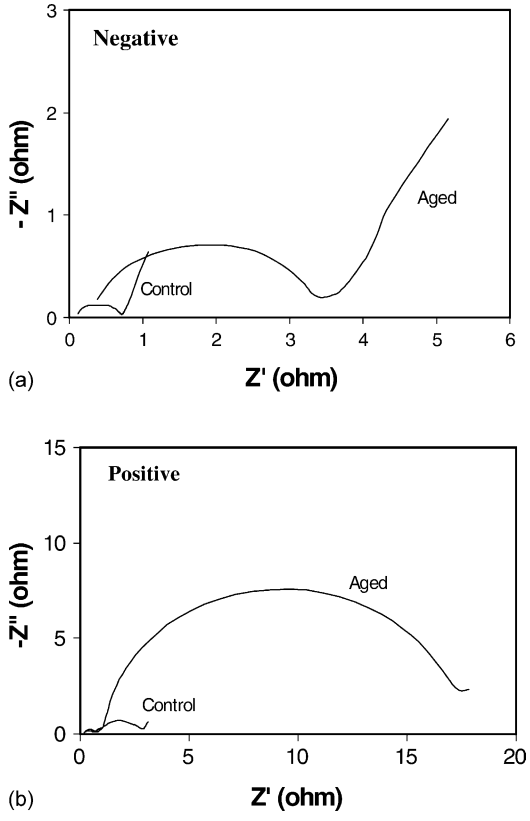

Fig. 2. Symmetric cell ac impedance data from (a) negative electrode and (b) positive electrode materials from aged (70 °C, 2 weeks) and control (formation only) 18650-cells.

that ASI values are higher for the aged materials. In addition, the positive electrode ASI increase is much larger than that of the negative electrode, which suggests that the positive electrode is the main contributor to the 18650-cell ASI increase. Representative symmetric cell data shows that the impedance increase of the positive electrodes is significantly greater than that of the negative electrodes (Fig. 2). Furthermore, the semi-circular arc at medium frequency, which is related to lithium-ion transport and charge-transfer kinetics at the positive electrode–electrolyte interface, increases significantly after accelerated aging.

3.2. Positive electrode coating characterization

Representative SEM images (Fig. 3) from fresh positive electrode laminates showed $LiNi_{0.8}Co_{0.2}O_2$ particles, graphite, acetylene black and the PVDF binder. Surface films, observed on laminates from control cells, were a mixture of electrolyte residue and electrode–electrolyte interaction products. Oxide particles from aged cells showed, in addition, particulate-type features (see Fig. 4), which appear to have resulted from localized reactions at the oxide surface.

Representative XPS spectra from fresh positive electrode laminates (see Fig. 5) showed peak intensities corresponding to (a) graphite and PVdF binder in the C 1s spectra, (b) $LiNi_{0.8}Co_{0.2}O_2$ and Li_2CO_3 peaks in the O 1s spectra, and (c) PVdF and LiF in the F 1s spectra; the LiF results from $LiNi_{0.8}Co_{0.2}O_2$ reaction with HF produced by dehydrofluorination in the binder during laminate preparation. Spectra from control samples showed additional intensities related to C–H, C–O and $–OCO_2$ peaks in the C 1s spectra, which are believed to arise from hydrocarbons (polymers), lithium alkoxides (ROLi) and lithium alkyl carbonates ($ROCO_2Li$); polycarbonates ($ROCO_2R'$) and polyethyleneoxide (PEO) are alternative possibilities. Intensities associated with PEO, ROLi, $ROCO_2Li$ and $ROCO_2R'$ were observed in the O 1s spectra. Relatively strong LiF peaks were observed in addition to PVdF peaks in the F 1s spectra, and intensities from Li_xPF_y- and Li_xPO_y-type compounds were seen in the P 2p spectra.

In general, the XPS peak profiles of aged samples were similar to those of the control samples. Furthermore, peak profiles of samples aged at 40, 50, 60, and 70 °C were similar, indicating that the same surface compounds were formed at the various test temperatures; representative data from the 70 °C samples are compared with the fresh sample spectra in Fig. 5. The peak locations were also unaffected by the calendar-life test duration and the cell voltage during aging.

In the O 1s spectra, the $LiNi_{0.8}Co_{0.2}O_2$ signal was relatively strong for the fresh sample but the intensity of this peak was either much lower or absent for the higher temperature samples. This decrease in peak intensity indicated

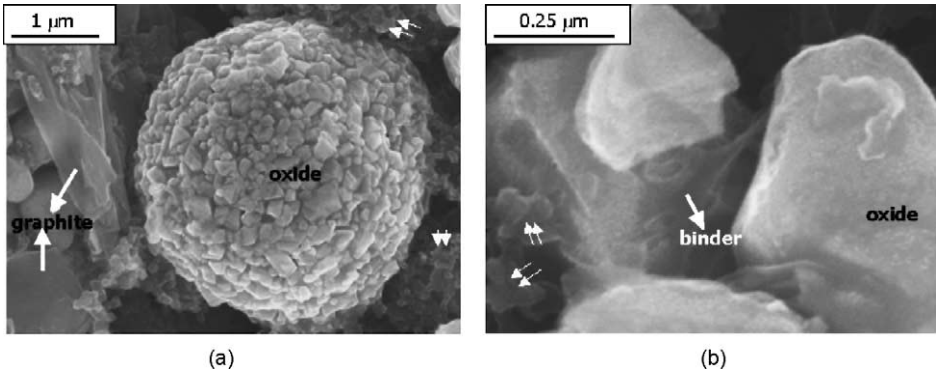

Fig. 3. Typical micrographs from a fresh positive electrode laminate showing (a) oxide, graphite and acetylene black (marked by double arrows), and (b) PVdF binder.

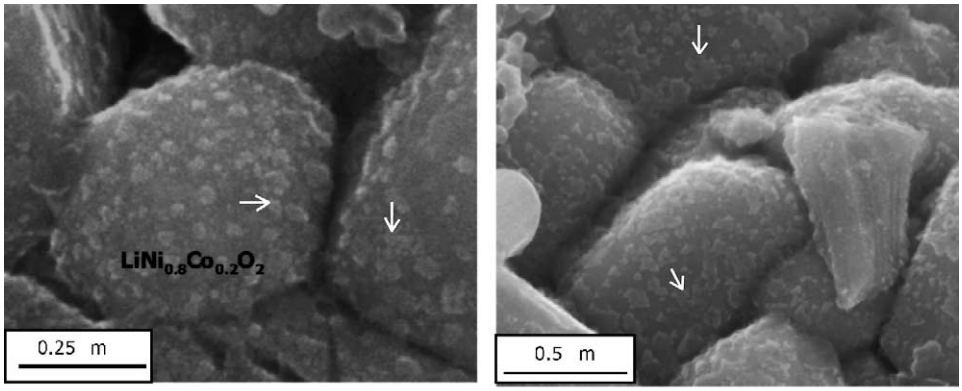

Fig. 4. Particulate-type features (marked by arrows) observed on surfaces of oxide particles in positive electrodes from (a) 40 °C calendar-life cell, (b) 70 °C, cycle-life cell.

the presence of a surface film on the $LiNi_{0.8}Co_{0.2}O_2$ particles that was thicker for the higher temperature samples. The absence of peak intensity for the 60 and 70 °C samples suggested that the surface film was thicker than the escape depth of photoelectrons originating from $LiNi_{0.8}Co_{0.2}O_2$. In contrast, the graphite peak at 284.5 eV in the C 1s spectra (see Fig. 5) was strong even for the aged samples. This difference between the graphite and $LiNi_{0.8}Co_{0.2}O_2$ peak intensities suggested that the $LiNi_{0.8}Co_{0.2}O_2$ particles were preferentially covered by surface films. An increase in surface film thickness, especially on the oxide particles, could have contributed to increased charge-transfer resistance at the cathode–electrolyte interface and hence to impedance rise measured in the aged cells.

The charge-transfer resistance increase could also have resulted from structural changes on the oxide particle surfaces [8]. High-resolution electron microscope (HREM) data have shown that $Li_xNi_{1-x}O$-type surface regions (NaCl structure) are present on the bulk layered (α-$NaFeO_2$ structure) material (see Fig. 6). These modified oxide surface layers were ~2–5 nm thick in samples from 0% power fade cells and >35 nm in samples from 43% power fade cells. This increase in thickness on cell aging could result from (a) occupation of Li layers by Co and Ni, and (b) oxygen loss from the surface regions by reactions with the electrolyte.

3.3. Negative electrode coating characterization

SEM images from a fresh negative electrode laminate showed the spherical MCMB graphite and the plate-like SFG graphite contained in the composite coating. The C 1s XPS spectra from the fresh laminate showed peaks from the graphites and PVdF binder. Samples from control cells did

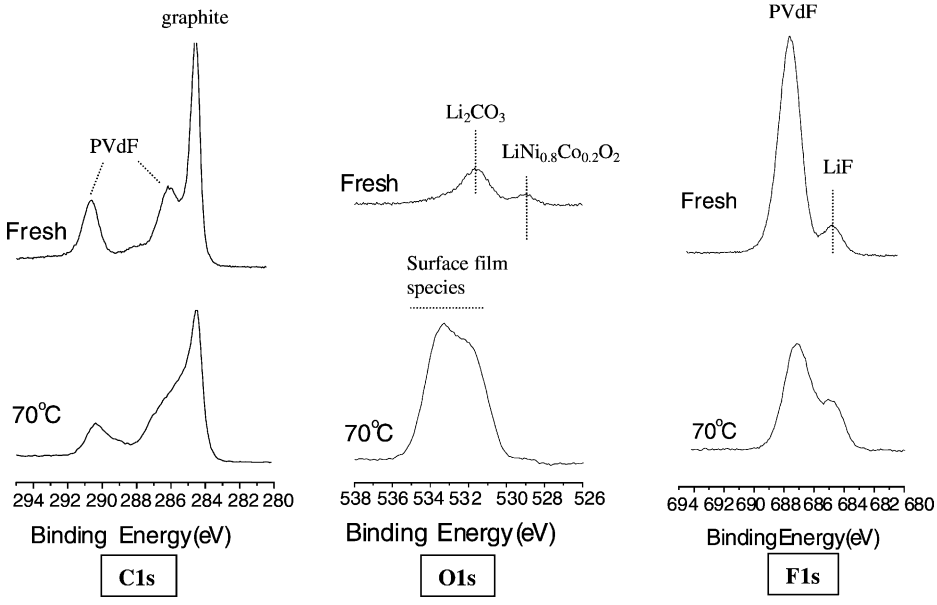

Fig. 5. Representative C 1s, O 1s and F 1s XPS spectra from fresh (no electrolyte contact) and aged (70 °C, 2 weeks) positive electrode laminates.

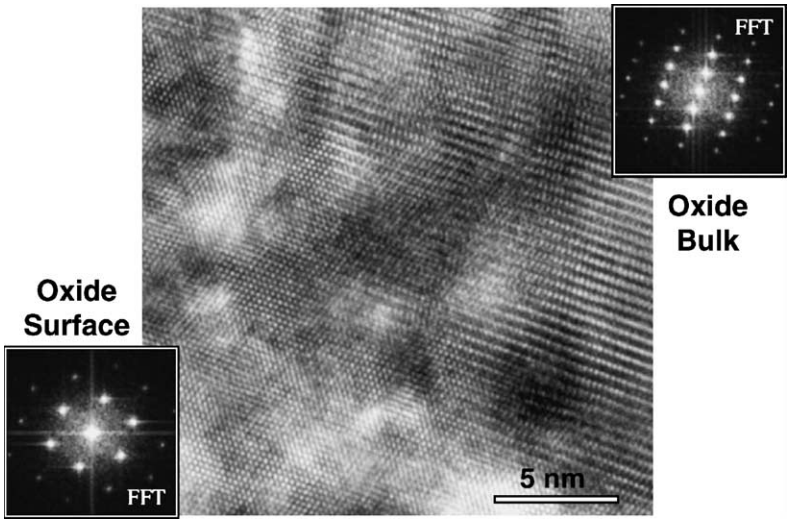

Fig. 6. HREM image of $LiNi_{0.8}Co_{0.2}O_2$ from a 43% power fade sample. The fast Fourier transform (FFT) patterns show clear differences between the bulk and near-surface regions.

not show the graphite peaks, which indicated the presence of an SEI layer; the thickness of this layer was greater than the escape depth of photoelectrons ejected from the graphite (~2 nm). The various XPS data [7] suggested that the SEI layers contained a mosaic of microphases, which included both solvent reduction products such as alkyl carbonates and ethoxides and salt reduction products such as LiF and Li_xPF_y. Species such as $LiPF_yO_z$, which could have formed from $LiPF_6$ decomposition and hydrolysis, and polymeric compounds such as PEO may also have been present in the SEI layers.

Samples from aged cells showed XPS spectra that were mostly similar to those from the control cells. The main differences were (a) strong Li_2CO_3 peaks in the C 1s spectra of aged samples, which could have resulted from the decomposition of lithium alkyl carbonates at the elevated storage temperatures, and (b) graphite peaks in the C 1s spectra of aged samples, which suggested that the original SEI layer had decomposed partially exposing some of the underlying graphite. The capacity fade observed in the cells could be the consequence of lithium consumption during the breakdown and reformation of the SEI layers.

3.4. Current collector characterization

Current collector samples from fresh, control and aged positive electrode laminates were examined to elucidate the role of Al pitting to cell power fade. SEM images from fresh laminates showed pits/mechanical indentations that resulted from the calendaring process. The size and density of pits in foils from cells aged at <50 °C were similar to those in the fresh laminate, which indicated that the impedance rise observed in these cells was not a result of foil pitting. Pit sizes and densities were significantly greater in samples aged at >60 °C; sample pitting may have contributed to impedance rise in these cells. Pits were not observed on negative electrode foil samples, which indicated that the copper current collector did not contribute to cell impedance rise.

3.5. Separator characterization

SEM studies were performed on separator samples to determine the contributions of separator degradation and/or plugging to cell power fade. A typical micrograph from a new separator sample showed both small and large pores through which the Li ions move during electrochemical cycling. Deposits were observed on unwashed separator samples from the aged cells, with more deposits on the anode side than on the cathode side. These deposits are believed to be surface layer remnants from the electrode materials that adhere to the separator during cell disassembly. The surface deposits were easily removed by washing the samples in a mixture of water and DMC. The pore size distribution of washed separator samples from aged cells were similar to the new separator sample. Furthermore, the ASI values for cells prepared with these aged-washed separator samples were similar to those obtained from cells employing new separators, which suggested that the separator contribution to 18650-cell power fade was very small.

3.6. Gas generation and electrolyte changes

The control cells contained hydrocarbon gases such as C_2H_6, CH_4, C_2H_2, C_2H_4 and a small amount of CO_2, which were generated during the formation process. Half-cell experiments with Gen 1 electrodes and Li metal indicated that a majority of these gases are generated at the negative, and are associated with electrolyte reduction and formation of the SEI layer. Cell gas volumes increased during accelerated aging. The CO_2 content and, especially, CO content of

the cells increased with aging temperature, which could have resulted from the breakdown and reformation of the SEI layer during cell aging.

The Gen 1 electrolyte formulation was 1 M $LiPF_6$ in 1:1 wt.% EC:DEC. Transesterification between EC and DEC produces ~4 wt.% diethyl-2,5-dioxahexanecarboxylate (DEDOHC) in the control cells. Quantitative analysis showed that the electrolyte compositions of aged cells were similar to those of control cells. The aging temperature, nominal cell voltage, and test period had little effect on the bulk electrolyte composition. It was evident that the electrode–electrolyte reactions, which produce SEI layers on the negative electrodes and surface films on the positive electrodes, produced little change in the bulk electrolyte.

4. Conclusions

A suite of diagnostic techniques was employed to determine the reasons for impedance rise and resulting power fade in lithium-ion cells. Electrochemical techniques, which employed both ac and dc measurements showed that the positive electrode was the main contributor to cell impedance rise during cell aging. Furthermore, the impedance rise was controlled by lithium-ion transport and charge-transfer kinetics at the positive electrode–electrolyte interface. This impedance rise may be correlated with surface film changes and crystal structure changes on the surface of $LiNi_{0.8}Co_{0.2}O_2$ particles. SEI layer changes may explain the slow impedance rise at the negative electrodes. The electrolyte indirectly contributes to impedance rise through its participation in reactions that produce surface films on the positive electrode and SEI layers on the negative electrode. The cell separator and the electrode current collectors are not likely contributors to cell impedance rise, especially at aging temperatures <50 °C.

Acknowledgements

The authors acknowledge the financial support of the US Department of Energy (DOE), Office of Advanced Automotive Technologies, under Contract No. W-31-109-ENG-38. The Center for Microanalysis of Materials at the University of Illinois is partially supported by DOE under grant DEFG02-96-ER45439. The authors are grateful to A. Andersson, A. Jansen and D. Dees for their contributions to this work. Work supported by the US Department of Energy, Office of Advanced Automotive Technologies, Office of Transportation Technologies, under Contract No. W-31-109-ENG-38.

References

[1] PNGV Battery Test Manual, Revision 2, Idaho National Engineering Laboratory, US Department of Energy, DOE/ID-10597, August 1999.
[2] I. Bloom, B.W. Cole, J.J. Sohn, S.A. Jones, E.G. Polzin, V.S. Battaglia, G.L. Henriksen, C. Motloch, R. Richardson, J. Power Sources 101 (2001) 238.
[3] X. Zhang, P.N. Ross Jr., R. Kostecki, F. Kong, S. Sloop, J.B. Kerr, K. Striebel, E.J. Cairns, F. McLarnon, J. Electrochem. Soc. 148 (2001) A463.
[4] M. Balasubramanian, X. Sun, X.Q. Yang, J. McBreen, J. Power Sources 92 (2001) 1.
[5] C.H. Chen, J. Liu, K. Amine, J. Power Sources 96 (2001) 321.
[6] K. Amine, C.H. Chen, J. Liu, M. Hammond, A. Jansen, D. Dees, I. Bloom, D. Vissers, G. Henriksen, J. Power Sources 97-98 (2001) 684.
[7] A.M. Andersson, D.P. Abraham, R. Haasch, S. MacLaren, J. Liu, K. Amine, J. Electrochem. Soc. 149 (2002) A1358.
[8] D.P. Abraham, R.D. Twesten, M. Balasubramanian, I. Petrov, J. McBreen, K. Amine, Electrochem. Commun. 4 (2002) 620.